Engineering qubit dynamics in open systems with photonic synthetic lattices

Francesco Di Colandrea [1,2,*] Tareq Jaouni [1] John Grace [1,3] Dilip Paneru [1] Mirko Arienzo [4] Alessio D'Errico [1,5] and Ebrahim Karimi [1,5,6]

[1]*Nexus for Quantum Technologies, University of Ottawa, Ottawa, Ontario K1N 5N6, Canada*
[2]*Dipartimento di Fisica "Ettore Pancini", Università degli Studi di Napoli Federico II, Complesso Universitario di Monte Sant'Angelo, Via Cintia, 80126 Napoli, Italy*
[3]*Department of Physics, McGill University, Montreal, Quebec H3A 0G4, Canada*
[4]*Institute for Quantum Inspired and Quantum Optimization, Hamburg University of Technology, Hamburg 21079, Germany*
[5]*National Research Council of Canada, 100 Sussex Drive, Ottawa, Ontario K1A 0R6, Canada*
[6]*Institute for Quantum Studies, Chapman University, Orange, California 92866, USA*

(Received 18 December 2024; accepted 11 May 2025; published 6 June 2025)

The evolution of a quantum system interacting with an environment can be described as a unitary process acting on both the system and the environment. In this framework, the system's evolution can be predicted by tracing out the environmental degrees of freedom. Here, we establish a precise mapping between the global unitary dynamics and the quantum operation involving the system, wherein the system is a single qubit, and the environment is modeled as a discrete lattice space. This approach enables the implementation of arbitrary noise operations on single-polarization qubits using a minimal set of three liquid-crystal metasurfaces, whose transverse distribution of the optic axes can be patterned to reproduce the target process. We experimentally validate this method by simulating common noise processes, such as phase errors and depolarization. Besides providing a practical solution for quantum state purification, this work demonstrates a versatile approach for the simulation of open qubit dynamics, with potential implications for quantum error correction and environment-induced quantum phase transitions.

DOI: 10.1103/PhysRevResearch.7.023236

I. INTRODUCTION

The majority of experiments in quantum mechanics require, to some extent, accounting for the influence of external effects over which the experimenter has limited knowledge or control. In this sense, any realistic quantum system should be regarded as an open system. Exposing a quantum system to an environment causes decoherence and dissipation, the main obstacle for hardware implementations of quantum computation protocols in the noisy intermediate-scale quantum (NISQ) era [1,2]. Surprisingly, decoherence can also represent a powerful resource in dissipation-driven quantum computation and state-engineering protocols [3,4].

From a quantum thermodynamics perspective, the interaction of one or few quantum bits with an environment involves exchanges of energy, work, and information [5–7]. Engineering qubit-environment interactions is thus a pivotal task for devising energy transfer processes, such as quantum heat engines [8–12], quantum batteries [13–16], and quantum refrigerators [17–20].

The capability of simulating these interactions also allows for addressing fundamental questions, for instance, in the context of emerging developments in understanding the interplay between geometric phases and quantum back action [21], wherein the variation of the geometrical phase has been demonstrated to be connected with the system-environment coupling strength in a topological fashion [22].

In recent years, it has also become common to describe open systems in terms of non-Hermitian processes, wherein the system evolution is dictated by a Hamiltonian operator that admits a complex spectrum, accounting for the possibility of gains and losses in subsets of modes [23–25]. Non-Hermitian dynamics have demonstrated a wide variety of applications in quantum physics [26–30] and photonics [31–33], in particular when exploiting phenomena related to the topological properties of the Hamiltonian [34–36]. The connection between the description of open systems as non-Hermitian processes and via master equations has been established [37], proving that it is generally possible to reduce the problem to a set of Kraus operators acting on the principal system [38].

Experimental setups where open dynamics can be simulated have recently been demonstrated. For example, the optical simulator presented in Ref. [39] uses a spatial light modulator to alter the polarization qubit of single photons in a programmable way, leveraging spatial multiplexing of the spectral degree of freedom to average over multiple realizations of the noisy channel in a single shot. On the other hand, the experiment reported in Ref. [40] demonstrates the

*Contact author: francesco.dicolandrea@unina.it

first simulation of open dynamics with continuous variables, assessed by measuring the spectral density [41] of the environmental coupling and the quantum non-Markovianity [42] of the process, with reconfigurability given by the possibility of rearranging complex networks of harmonic oscillators in various tailored structures [43]. However, these studies only focused on the reduced dynamics of the system, without establishing a clear connection with the global (system-environment) unitary. In this work, we demonstrate a step forward in this direction. We realize a platform where arbitrary sets of Kraus operators acting on a single qubit can be implemented, thus allowing for the simulation of any noise operator. Our strategy is based on coupling the qubit with an environment modeled as an infinite, discrete set of modes, visualized as a one-dimensional (1D) lattice space. By leveraging translational invariance, we derive an effective relation between the global unitary and the target set of Kraus operators. Once such a unitary is identified, it can be implemented in a compact photonic circuit consisting of a stack of three patterned wave plates [44]. In so doing, we can implement arbitrary operations on light polarization, encoding the qubit, by coupling it with the transverse spatial degree of freedom. This method is validated in a proof-of-principle experiment where we simulate common noise processes with different strengths.

Our results demonstrate that this approach could also be employed to benchmark quantum thermal machines' functionality and test the fundamental properties of open quantum systems.

II. RESULTS

The dynamics of a quantum system (here, a single qubit) is most generally described by a quantum channel $\mathcal{N}$, describing the noisy evolution of the system, that maps an input state $\rho_{\rm in}$ into the final state $\rho_{\rm f} = \mathcal{N}(\rho_{\rm in})$. Mathematically, $\mathcal{N}$ corresponds to a completely positive, trace-preserving map, which can be specified by a set of Kraus operators $\{A_k\}$ such that

$$\rho_{\rm f} = \sum_k A_k \rho_{\rm in} A_k^\dagger, \tag{1}$$

under the trace-preserving condition $\sum_k A_k A_k^\dagger = \sigma_0$, where σ_0 is the 2×2 identity operator [38]. An equivalent description is to consider the qubit as a system S interacting with an environment E. The qubit and environment define a closed system $\Omega = S + E$, described by a pure state undergoing a unitary evolution [see Fig. 1(a)]. This corresponds to choosing a *purification* of the system S. The choice of purification (or, equivalently, of the environment E) is not unique [38]. We will show in the following that it is always possible to model the environment as an infinite-dimensional Hilbert space $\mathcal{H}_E$ spanned by a discrete set of states $\{|m\rangle\}$, with $m \in \mathbb{Z}$. These states can be interpreted as the eigenstates of the position operator on an infinite 1D lattice. This suggests that the system-environment interaction occurs in the form of a translation-invariant unitary operator U. Accordingly, the latter can be block-diagonalized in the reciprocal space

$$U = \int_0^{2\pi} \mathrm{d}q\, \mathcal{U}(q)|q\rangle\langle q|, \tag{2}$$

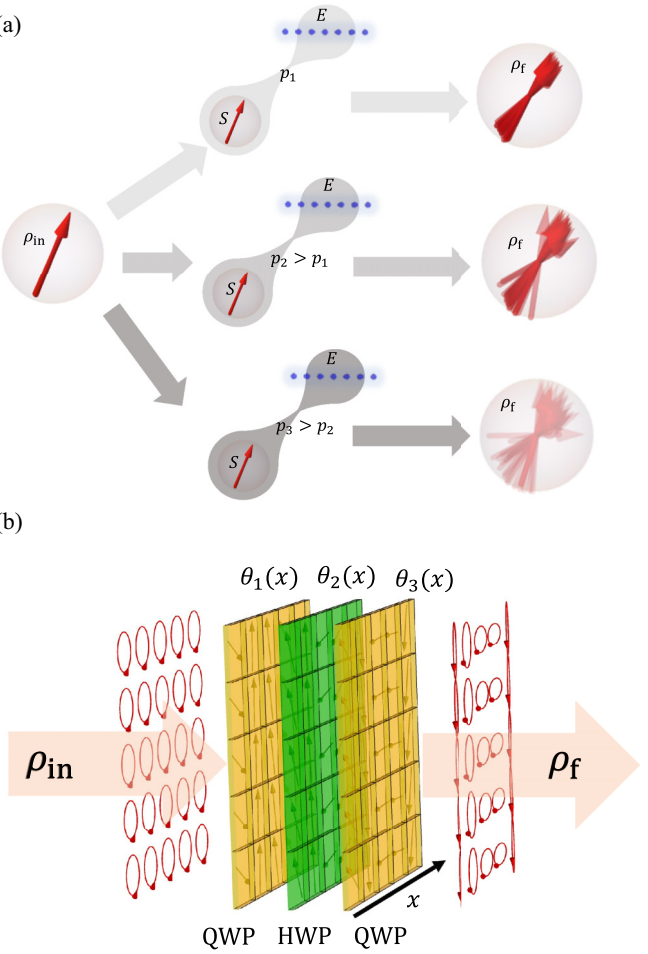

FIG. 1. Concept of the experiment. (a) A qubit initialized in a pure state $\rho_{\rm in}$ interacts with an external environment (E) featuring discrete lattice symmetry. The interaction strength is controlled by the parameter p, which can be tuned to produce different output mixed states $\rho_{\rm f}$. Larger values of p imply that the final state is delocalized over a larger number of lattice sites, leading to a reduction in the qubit state purity. (b) Our approach relies on the use of three liquid-crystal metasurfaces, each characterized by an optic-axis pattern $\theta_i(x)$, where x encodes the position reciprocal coordinate via the mapping $x = \Lambda q/(2\pi)$, with Λ a characteristic spatial period. In this implementation, the qubit is encoded into light polarization and the metasurfaces implement the system-environment interaction as a polarization-position coupling.

where $|q\rangle := \sum_m \exp(iqm)|m\rangle/\sqrt{2\pi}$ is a quasimomentum eigenstate and $\mathcal{U}(q)$ is an SU(2) operator that acts on the Hilbert space of the qubit $\mathcal{H}_S$.

Without loss of generality, we can assume that the environment is initialized in a pure state $\rho_{E,\rm in} = |m = 0\rangle\langle m = 0|$, so that the global initial state is $\rho_{\Omega,\rm in} = \rho_{S,\rm in} \otimes \rho_{E,\rm in}$. This assumption is typically verified in most experimental settings. Applying U to the input state, we obtain the following:

$$\begin{aligned}\rho_{\Omega,\rm f} &= U \rho_{\Omega,\rm in} U^\dagger \\ &= \frac{1}{2\pi} \iint \mathrm{d}q\, \mathrm{d}q'\, \mathcal{U}(q)\rho_{S,\rm in}\mathcal{U}^\dagger(q')|q\rangle\langle q'|,\end{aligned} \tag{3}$$

where the integrals are taken over the interval $[0, 2\pi]$. After the interaction, the state of the qubit can be retrieved by taking the partial trace of the evolved density operator with respect to the environment in the quasimomentum representation:

$$\rho_{\rm f} = \mathrm{tr}_E(\rho_{\Omega,\rm f}) = \int_0^{2\pi} \mathrm{d}q\, \langle q|\rho_{\Omega,\rm f}|q\rangle = \frac{1}{2\pi}\int_0^{2\pi} \mathrm{d}q\, \mathcal{U}(q)\rho_{\rm in}\mathcal{U}^\dagger(q), \tag{4}$$

where the system label S has been omitted. Our goal is to design $\mathcal{U}(q)$ such that the evolved density operator $\rho_{\rm f}$ of the qubit is equivalent to the outcome of a target noise operation $\mathcal{N}$. Mathematically, this corresponds to solving

$$\frac{1}{2\pi}\int_0^{2\pi} \mathrm{d}q\, \mathcal{U}(q)\rho_{\rm in}\mathcal{U}^\dagger(q) = \sum_k A_k \rho_{\rm in} A_k^\dagger, \tag{5}$$

under the constraint that $\mathcal{U}(q)$ is an SU(2) matrix at each q.

To this aim, we decompose $\mathcal{U}(q)$ and each Kraus operator A_k into linear combinations of the identity and Pauli matrices $(\sigma_1, \sigma_2, \sigma_3)$, a set of complete basis for the 2×2 matrices:

$$\begin{aligned}\mathcal{U}(q) &= u_0(q)\sigma_0 - i(u_1(q)\sigma_1 + u_2(q)\sigma_2 + u_3(q)\sigma_3),\\ A_k &= c_0^{(k)}\sigma_0 - i\big(c_1^{(k)}\sigma_1 + c_2^{(k)}\sigma_2 + c_3^{(k)}\sigma_3\big),\end{aligned} \tag{6}$$

which yields [see Eq. (5)]

$$\sum_{i,j}\frac{1}{2\pi}\int_0^{2\pi} \mathrm{d}q\, u_i(q)u_j(q)\sigma_i\sigma_j = \sum_{i,j}\sum_k c_i^{(k)}c_j^{*(k)}\sigma_i\sigma_j, \tag{7}$$

where $*$ denotes complex conjugation. Equation (7) corresponds to a system of 16 equations of the following form:

$$\frac{1}{2\pi}\int_0^{2\pi} \mathrm{d}q\, u_i(q)u_j(q) = \sum_k c_i^{(k)}c_j^{*(k)}, \tag{8}$$

for $\{i, j\} = 0, 1, 2, 3$, that can be solved numerically for the coefficients $\{u_i(q)\}$ under the unitary constraint

$$u_0^2(q) + u_1^2(q) + u_2^2(q) + u_3^2(q) = 1, \tag{9}$$

for all $q \in [0, 2\pi]$ (see Methods for details). Importantly, the solution holds for any qubit initialization; therefore, we engineer an effective simulation of the target noise.

Once the global unitary has been identified, an experimental setting can be created to implement such an operator. In our photonic setup, the qubit is encoded into light polarization, while the environment state $|m\rangle$ corresponds to an optical mode carrying m units of transverse momentum $\Delta k_\perp = 2\pi/\Lambda$, where Λ is a characteristic length comparable with the beam radius. This corresponds to mapping the quasimomentum coordinate into the photon transverse position: $q = 2\pi x/\Lambda$ [45]. With this encoding scheme, arbitrary unitary operators in the form of Eq. (2) can be simulated using a minimal stack of three patterned wave plates [see Fig. 1(b)]. This technique has been introduced in Ref. [44] as a compact solution to simulate ultralong quantum walks. It is well known that a sequence of a half-wave plate (HWP) sandwiched between two quarter-wave plates (QWPs) can implement an arbitrary polarization transformation by adjusting the orientation of the optic axes θ_i of each wave plate [46]. In the circular polarization basis, where $|L\rangle := (1, 0)^T$ and $|R\rangle := (0, 1)^T$ are the left and right circular polarization states, respectively, and T stands for transpose, the general transformation matrix associated with a wave plate can be written as

$$W_i(\theta_i) = \cos\left(\frac{\delta_i}{2}\right)\sigma_0 + i\sin\left(\frac{\delta_i}{2}\right)(\cos(2\theta_i)\sigma_1 + \sin(2\theta_i)\sigma_2), \tag{10}$$

where the subscript $i = 1, 2, 3$ labels individual wave plates, $\delta_1 = \delta_3 = \pi/2$ are the optical retardations of the QWPs W_1 and W_3, $\delta_2 = \pi$ is the retardation of the HWP W_2, and θ_i are the optic-axis orientation angles. The required patterns $\theta_i(x)$ can be determined by solving $W_3W_2W_1 = \mathcal{U}$ at each q (see Methods). Patterned wave plates are fabricated as electrically tunable nematic liquid-crystal metasurfaces, with the optic axis locally patterned via a well-established photoalignment technique [47].

We demonstrate our approach by fabricating stacks of plates simulating different instances of quantum noise, specifically, phase flip, bit flip, bit-phase flip, and depolarization channels. These are defined by the following sets of Kraus operators. For the first three channels, $A_0 = \sqrt{1-p}\,\sigma_0$ and $A_1 = \sqrt{p}\,\sigma_i$, with $i = 1, 2, 3$ for bit flip, bit-phase flip, and phase flip, respectively. The depolarization channel is instead characterized by the Kraus operators $\{A_0, A_1, A_2, A_3\}$, where $A_0 = \sqrt{1-p}\,\sigma_0$ and $A_i = \sqrt{p/3}\,\sigma_i$ [38]. Each channel has been implemented for three values of the system-environment coupling parameter, $p = 1/8,\ 1/4,\ 1/2$, corresponding to the weak, intermediate, and strong interaction regimes, respectively [48]. The coupling parameter physically represents the probability that a certain Pauli gate is applied to the qubit system. Intuitively, higher values of p are associated with processes in which a larger number of lattice sites are occupied, each with a different polarization. This results in greater uncertainty in the definition of the final qubit state, thereby leading to a reduction in its purity.

The experimental setup is outlined in Fig. 2(a). An 810 nm laser beam crosses a state-preparation stage consisting of a polarizer (P), a half-wave plate (H), and a quarter-wave plate (Q). For each noise realization, we choose as input states $|L\rangle$, $|H\rangle$, and $|D\rangle$, where $|H\rangle = (|L\rangle + |R\rangle)/\sqrt{2}$ and $|D\rangle = (|L\rangle + i|R\rangle)/\sqrt{2}$ are the horizontal and diagonal polarization states, respectively. The noise $\mathcal{N}$ is implemented by three liquid-crystal metasurfaces $W_1 - W_2 - W_3$. The output qubit-polarization state is analyzed with a sequence Q–H–P, measuring the transmitted intensity with a power-meter detector (D). This allows us to retrieve the three Stokes parameters providing the representation of the qubit state on the Bloch sphere [49]. The optic-axis patterns of the metasurfaces used to simulate phase flip, bit flip, and bit-phase flip are plotted in Fig. 2(b). These channels feature the same Kraus operators decomposition up to a basis rotation that can be implemented with uniform wave plates, and can therefore be simulated with the same sets of plates. The patterns for the depolarization channels are provided in Fig. 2(c). It is evident that the complexity of the patterns increases with the complexity

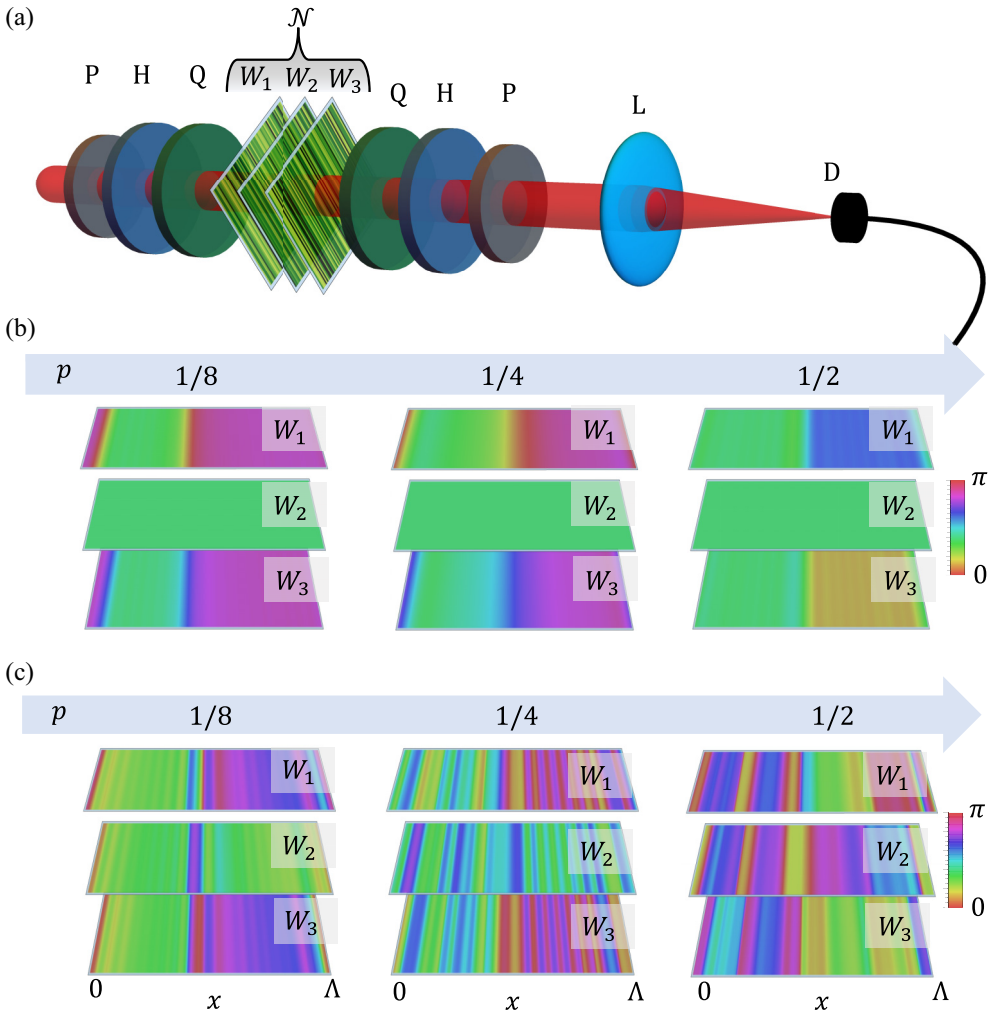

FIG. 2. Experimental setup. (a) Sketch of the experimental setup. P: polarizer, H: half-wave plate, Q: quarter-wave plate, L: lens, D: detector. The noise $\mathcal{N}$ is implemented by a sequence of three liquid-crystal metasurfaces $W_1 - W_2 - W_3$. In our experiment, we set $\Lambda = 2.5$ mm. The input beam waist was $w_0 \simeq \Lambda$, corresponding to a pure localized environment. (b) Optic-axis patterns of the plates used for phase flip, bit flip, and bit-phase flip, for different values of the coupling parameter p. (c) Patterns for the depolarization channel. The hue color coding indicates the orientation $\theta(x)$ of the liquid-crystal optic axis on the metasurfaces plane.

of the simulated interaction. This is due to higher-frequency modulations required to couple the qubit to a larger number of lattice sites.

The experimental results are illustrated in Fig. 3, where we plot the measured Stokes parameters [see Fig. 3(a)] and the corresponding trajectories [see Fig. 3(b)] of the qubit states on the Bloch sphere as a function of the noise level p. Deviations from the theory are systematic errors due to imperfect alignment of the plates and fabrication defects, in agreement with Monte Carlo simulations whose results are reported as error bands around the theoretical lines in Fig. 3(a). Overall, the average fidelity $\mathcal{F} = \mathrm{Tr}(\sqrt{\sqrt{\rho_{\mathrm{th}}}\rho_{\mathrm{exp}}\sqrt{\rho_{\mathrm{th}}}})^2$ between the measured states ρ_{exp} and the expected ones ρ_{th} is always above 98%, proving that our devices reproduce the target channels with high accuracy. The results for phase flip, bit flip, and bit-phase flip show that the action of the noise keeps unaltered the qubit states initialized in the eigenstate of A_1, while it pushes other inputs toward the origin of the Bloch sphere. The depolarization channel displays similar behavior for all pure input states [38].

III. CONCLUSIONS

In this work, we demonstrated a general approach for engineering noise operations on a qubit system, based on suitably coupling the qubit with a lattice-like environment. We provided a systematic procedure for constructing a global unitary operator corresponding to the desired process on the qubit state. In our photonic demonstration, light polarization played the role of a qubit, and the environment was encoded into a set of transverse modes, with the interaction occurring in the form of a space-dependent polarization transformation, engineered via liquid-crystal metasurfaces. The patterns of the metasurfaces have been inverse-designed to simulate typical noise operations in different interaction regimes.

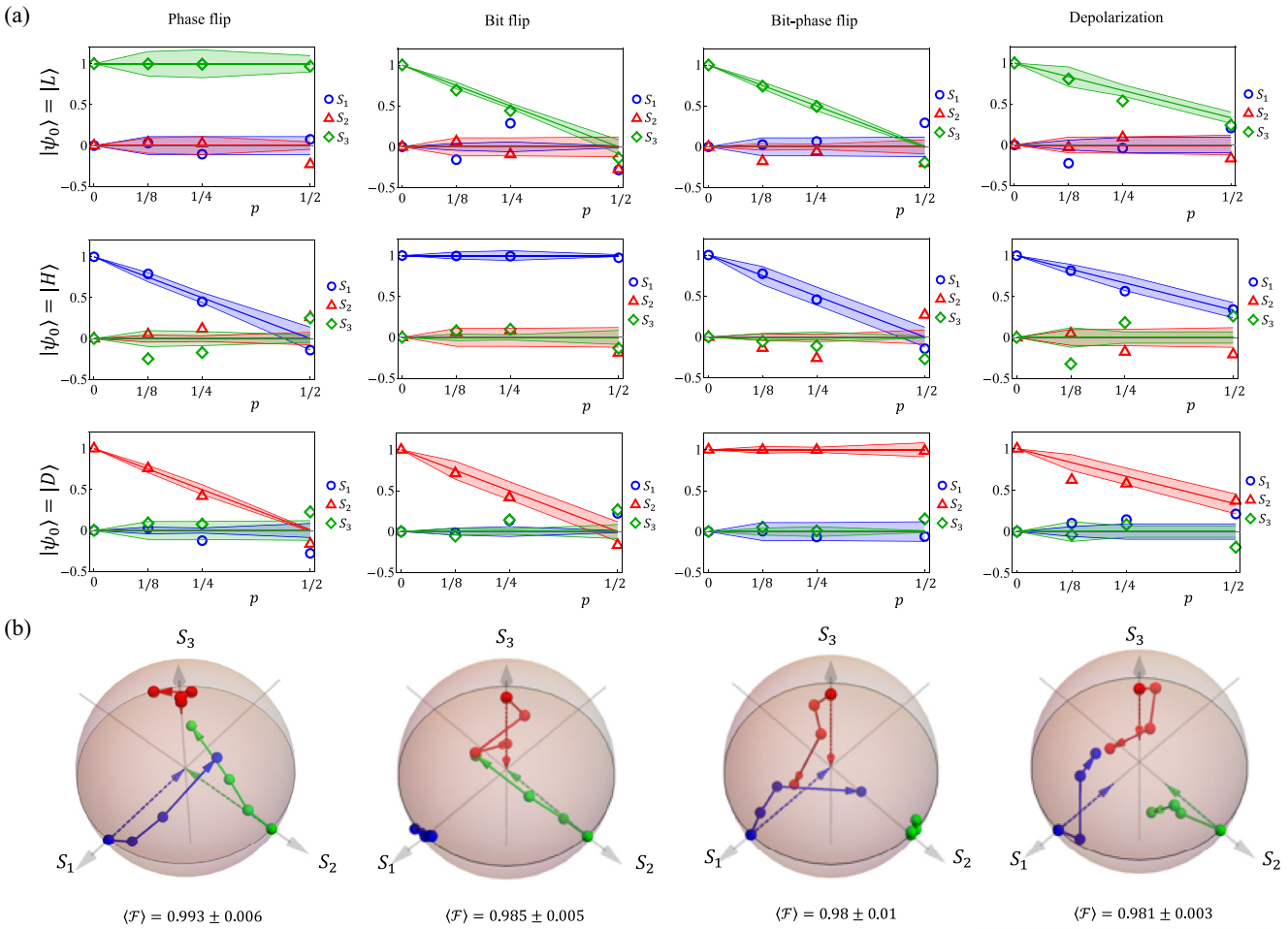

FIG. 3. Experimental results. (a) Output qubit states in terms of the measured Stokes parameters S_1, S_2, S_3 (empty markers), with varying coupling strength p. The $p = 0$ case is included as a guide and corresponds to the nominal input state. Continuous lines show the theoretical trends, with error bands representing confidence intervals accounting for experimental imperfections. The latter have been evaluated with Monte Carlo simulations, where the relative alignment of the plates and their optical retardation have been considered as Gaussian random variables with a 5% standard deviation, estimated through direct measurements on fabricated samples. The bands are the standard deviations on the Stokes parameters extracted from 100 realizations of simulated experiments. Results are shown for the processes of phase flip, bit flip, bit-phase flip, and depolarization, with three different pure input states, $|H\rangle$, $|D\rangle$, and $|L\rangle$, respectively oriented along the S_1, S_2, and S_3 axis of the Bloch sphere. (b) Qubit trajectories (as function of p) on the Bloch sphere. Dashed arrows are the theoretical predictions, while joined spheres are the experimental results. Different colors correspond to different input states: $|H\rangle$ (blue), $|D\rangle$ (green), and $|L\rangle$ (red). In the insets, we report the average fidelities between the reconstructed and expected states.

Our findings pave the way for innovative solutions for studying open quantum systems. While in this work we focused on standard, well-known examples of quantum noise, our platform can readily be adapted to simulate arbitrary qubit-environment interactions. Potential applications involve the simulations of quantum machines, such as quantum refrigerators, protocols of quantum thermodynamics, chiral dynamics in open systems, as well as geometric-phase and topological effects in non-Hermitian evolutions. Furthermore, such controlled and high-fidelity simulations of common forms of noise could foster the development of effective strategies for quantum error correction [50] or alternative protocols of dissipation-driven quantum computation [3]. In the future, the trace-preserving assumption could be relaxed by post-selecting only a subset of lattice sites following the qubit-environment interaction. Another interesting prospect concerns the generalization of our scheme to a larger number of qubits, where the emerging concepts of local passivity [51] and ergotropy [52,53] could be experimentally observed. Nevertheless, the same setup could still be used to investigate the effects of known single-qubit noises on single- and multi-mode entangled states, monitoring how different noises degrade nonlocal correlations [54]. Conversely, this work could also stimulate theoretical research on environment-assisted quantum process tomography of nonunitary channels [55,56], where one probes the environment to gain information on the (unknown) system dynamics. Finally, by replacing liquid-crystal metasurfaces with spatial light modulators, our setup could be made reconfigurable in real-time, which is an ideal feature for experimentally investigating dynamical

phenomena such as environment-induced quantum phase transitions [57,58].

IV. METHODS

A. Numerical optimization

To solve the system of equations given by Eq. (8), we expand each coefficient $\{u_i(q)\}$ in the Fourier basis:

$$u_i(q) = u_i^{(0)} + \sum_{n=1}^{N} \left(u_{ic}^{(n)} \cos(nq) + u_{is}^{(n)} \sin(nq)\right), \tag{11}$$

where N is the maximum number of spatial frequencies which can be tuned. By substituting the decomposition of Eq. (11) into Eq. (8), and performing the corresponding integrals, we obtain a simple relation for the Fourier coefficients:

$$2u_i^{(0)}u_j^{(0)} + \sum_{n=1}^{N}\left(u_{ic}^{(n)}u_{jc}^{(n)} + u_{is}^{(n)}u_{js}^{(n)}\right) = 2\sum_k c_i^{(k)}c_j^{*(k)}, \tag{12}$$

for $\{i, j\} = 0, 1, 2, 3$. The system of equations given by Eq. (12) can be solved numerically, under the unitary constraint $u_0^2(q) + u_1^2(q) + u_2^2(q) + u_3^2(q) = 1$ at each quasi-momentum value. To accomplish this, an iterative solution is adopted. First, we discretize the interval $[0, 2\pi]$ in $Q = 125$ points. This value is chosen to ensure a dense sampling of the spatial period. Then, we numerically minimize the following cost function for the Fourier coefficients:

$$f_1 = \sum_{i,j}\left[2u_i^{(0)}u_j^{(0)} + \sum_{n=1}^{N}\left(u_{ic}^{(n)}u_{jc}^{(n)} + u_{is}^{(n)}u_{js}^{(n)}\right) - 2\sum_k c_i^{(k)}c_j^{*(k)}\right]^2. \tag{13}$$

The solutions of the first minimization routine are used as input guesses for the minimization of a second cost function, expressing the unitary constraint at each (discretized) quasi-momentum value:

$$f_2 = \sum_{i=1}^{Q}\left(u_0^2(q_i) + u_1^2(q_i) + u_2^2(q_i) + u_3^2(q_i) - 1\right)^2. \tag{14}$$

The second minimization output feeds the previous minimization routine for the cost function f_1, and so forth, until the total difference between the optimized coefficients from the two routines is less than 10^{-12} or when the number of iterations reaches $T = 200$, whichever occurs first. This systematically allowed us to minimize both cost functions to values of order $\approx 10^{-12}$, by enforcing only $N = 20$ frequencies. As detailed in the next section, the maximum number of spatial frequencies determines the complexity of the plates to be fabricated, therefore, it is desirable to achieve a solution with a reasonably small number of frequencies.

B. Extracting the metasurfaces' patterns

The nested minimization routines described above output an optimal set of Fourier coefficients for a given noise, which in turn determines the space-dependent unitary operator U in the form of Eq. (2). After the identification $q \leftrightarrow x$, at each transverse position, the operator U implements a polarization rotation $\mathcal{U}(x)$ of an angle χ around the axis $\mathbf{n} = (n_1, n_2, n_3)$:

$$\mathcal{U}(x) = \cos\left(\frac{\chi(x)}{2}\right)\sigma_0 - i\sin\left(\frac{\chi(x)}{2}\right)\mathbf{n}(x)\cdot\boldsymbol{\sigma}, \tag{15}$$

where $\boldsymbol{\sigma} = \{\sigma_1, \sigma_2, \sigma_3\}$, and

$$\begin{aligned}\chi &= 2\arccos u_0;\\ n_i &= \frac{u_i}{\sin\left(\frac{\chi}{2}\right)},\end{aligned} \tag{16}$$

for $i = 1, 2, 3$ [cf. Eq. (6)].

The optical sequence of three liquid-crystal metasurfaces $\mathcal{L} = W_3(\theta_3)W_2(\theta_2)W_1(\theta_1)$ can be analogously decomposed as

$$\mathcal{L}(x) = \ell_0(x)\sigma_0 - i(\ell_1(x)\sigma_1 + \ell_2(x)\sigma_2 + \ell_3(x)\sigma_3), \tag{17}$$

where

$$\begin{aligned}\ell_0 &= -\cos\alpha\cos\beta,\\ \ell_1 &= -\sin\beta\sin\gamma,\\ \ell_2 &= \sin\beta\cos\gamma,\\ \ell_3 &= \sin\alpha\cos\beta,\end{aligned} \tag{18}$$

with $\alpha = \theta_1 - \theta_3$, $\beta = \theta_1 - 2\theta_2 + \theta_3$, and $\gamma = \theta_1 + \theta_3$. The dependence on the transverse coordinate x is omitted for ease of notation. Imposing $\mathcal{U} = \mathcal{L}$ at each transverse position yields

$$\cos\alpha\cos\beta = -\cos\frac{\chi}{2}, \tag{19a}$$

$$\sin\beta\sin\gamma = -\sin\frac{\chi}{2}\sin\vartheta\cos\varphi, \tag{19b}$$

$$\sin\beta\cos\gamma = \sin\frac{\chi}{2}\sin\vartheta\sin\varphi, \tag{19c}$$

$$\sin\alpha\cos\beta = \sin\frac{\chi}{2}\cos\vartheta, \tag{19d}$$

where we used the spherical parametrization of the vector $\mathbf{n}$: $n_1 = \sin\vartheta\cos\varphi$, $n_2 = \sin\vartheta\sin\varphi$, and $n_3 = \cos\vartheta$.

From Eqs. (19b) and (19c), it follows

$$\gamma = \varphi - \frac{\pi}{2}. \tag{20}$$

Two sets of solutions are found from Eqs. (19a) and (19d):

$$\begin{aligned}\alpha_1 &= \mathrm{atan2}\left(-\sin\frac{\chi}{2}\cos\vartheta, \cos\frac{\chi}{2}\right)\\ \beta_1 &= \mathrm{atan2}\left(\sin\frac{\chi}{2}\sin\vartheta, -\sqrt{1-\sin^2\frac{\chi}{2}\sin^2\vartheta}\right)\\ \gamma_1 &= \varphi - \pi/2\end{aligned} \tag{21}$$

$$\begin{aligned}\alpha_2 &= \pi + \alpha_1\\ \beta_2 &= \pi - \beta_1\\ \gamma_2 &= \gamma_1\end{aligned} \tag{22}$$

where $\mathrm{atan2}(x, y)$ is the two-argument arctangent function, which distinguishes between diametrically opposite directions. From the expressions for α, β, and γ, the modulations

for the metasurfaces' optic-axis patterns θ_1, θ_2, and θ_3 can be finally extracted. A modulation obtained from a single set of solutions may exhibit discontinuities. To avoid this issue, a dedicated routine automatically switches the solution to be picked whenever the values of the angles feature a sudden jump [44].

ACKNOWLEDGMENTS

This work was supported by Canada Research Chairs (CRC) and Quantum Enhanced Sensing and Imaging (QuEnSI) Alliance Consortia Quantum grant. F.D.C. further acknowledges support from the PNRR MUR Project (No. PE0000023-NQSTI).

F.D.C. conceived the idea and developed the theory, with contributions from A.D.E. and M.A. F.D.C., T.J., and J.G. fabricated the metasurfaces. F.D.C., J.G., and D.P. performed the experiment. F.D.C., T.J., and J.G. analyzed the data. F.D.C. and A.D.E. prepared the first version of the manuscript. A.D.E. and E.K. supervised the project.

The authors declare no conflicts of interest.

DATA AVAILABILITY

The data that support the findings of this article are not publicly available. The data are available from the authors upon reasonable request.

[1] J. Preskill, Quantum Computing in the NISQ era and beyond, Quantum **2**, 79 (2018).
[2] E. Campbell, A series of fast-paced advances in quantum error correction, Nat. Rev. Phys. **6**, 160 (2024).
[3] F. Verstraete, M. M. Wolf, and J. I. Cirac, Quantum computation and quantum-state engineering driven by dissipation, Nat. Phys. **5**, 633 (2009).
[4] P. M. Harrington, E. J. Mueller, and K. W. Murch, Engineered dissipation for quantum information science, Nat. Rev. Phys. **4**, 660 (2022).
[5] R. Kosloff, Quantum thermodynamics: A dynamical viewpoint, Entropy **15**, 2100 (2013).
[6] S. Vinjanampathy and J. Anders, Quantum thermodynamics, Contemp. Phys. **57**, 545 (2016).
[7] S. Deffner and S. Campbell, *Quantum Thermodynamics*, 2053-2571 (Morgan & Claypool Publishers, San Rafael, CA, 2019).
[8] M. O. Scully, Extracting work from a single thermal bath via quantum negentropy, Phys. Rev. Lett. **87**, 220601 (2001).
[9] H.-T. Quan, Y.-X. Liu, C.-P. Sun, and F. Nori, Quantum thermodynamic cycles and quantum heat engines, Phys. Rev. E **76**, 031105 (2007).
[10] M. O. Scully, K. R. Chapin, K. E. Dorfman, M. B. Kim, and A. Svidzinsky, Quantum heat engine power can be increased by noise-induced coherence, Proc. Natl. Acad. Sci. USA **108**, 15097 (2011).
[11] O. Fialko and D. W. Hallwood, Isolated quantum heat engine, Phys. Rev. Lett. **108**, 085303 (2012).
[12] J. P. S. Peterson, T. B. Batalhao, M. Herrera, A. M. Souza, R. S. Sarthour, I. S. Oliveira, and R. M. Serra, Experimental characterization of a spin quantum heat engine, Phys. Rev. Lett. **123**, 240601 (2019).
[13] R. Alicki and M. Fannes, Entanglement boost for extractable work from ensembles of quantum batteries, Phys. Rev. E **87**, 042123 (2013).
[14] F. C. Binder, S. Vinjanampathy, K. Modi, and J. Goold, Quantacell: powerful charging of quantum batteries, New J. Phys. **17**, 075015 (2015).
[15] F. Campaioli, S. Gherardini, J. Q. Quach, M. Polini, and G. M. Andolina, Colloquium: quantum batteries, Rev. Mod. Phys. **96**, 031001 (2024).
[16] A. G. Catalano, S. M. Giampaolo, O. Morsch, V. Giovannetti, and F. Franchini, Frustrating quantum batteries, PRX Quantum **5**, 030319 (2024).
[17] R. Kosloff, E. Geva, and J. M. Gordon, Quantum refrigerators in quest of the absolute zero, J. Appl. Phys. **87**, 8093 (2000).
[18] A. Levy, R. Alicki, and R. Kosloff, Quantum refrigerators and the third law of thermodynamics, Phys. Rev. E **85**, 061126 (2012).
[19] N. Brunner, M. Huber, N. Linden, S. Popescu, R. Silva, and P. Skrzypczyk, Entanglement enhances cooling in microscopic quantum refrigerators, Phys. Rev. E **89**, 032115 (2014).
[20] L. A. Correa, J. P. Palao, D. Alonso, and G. Adesso, Quantum-enhanced absorption refrigerators, Sci. Rep. **4**, 3949 (2014).
[21] Y.-W. Cho, Y. Kim, Y.-H. Choi, Y.-S. Kim, S.-W. Han, S.-Y. Lee, S. Moon, and Y.-H. Kim, Emergence of the geometric phase from quantum measurement back-action, Nat. Phys. **15**, 665 (2019).
[22] M. F. Ferrer-Garcia, K. Snizhko, A. D'Errico, A. Romito, Y. Gefen, and E. Karimi, Topological transitions of the generalized pancharatnam-berry phase, Sci. Adv. **9**, eadg6810 (2023).
[23] N. Moiseyev, *Non-Hermitian Quantum Mechanics* (Cambridge University Press, 2011).
[24] Y. Ashida, Z. Gong, and M. Ueda, Non-Hermitian physics, Adv. Phys. **69**, 249 (2020).
[25] N. Hatano and D. R. Nelson, Vortex pinning and non-Hermitian quantum mechanics, Phys. Rev. B **56**, 8651 (1997).
[26] N. Hatano and D. R. Nelson, Localization transitions in non-Hermitian quantum mechanics, Phys. Rev. Lett. **77**, 570 (1996).
[27] R. Hamazaki, K. Kawabata, and M. Ueda, Non-Hermitian many-body localization, Phys. Rev. Lett. **123**, 090603 (2019).
[28] E. Lee, H. Lee, and B.-J. Yang, Many-body approach to non-Hermitian physics in fermionic systems, Phys. Rev. B **101**, 121109(R) (2020).
[29] K. Kawabata, K. Shiozaki, and S. Ryu, Many-body topology of non-Hermitian systems, Phys. Rev. B **105**, 165137 (2022).
[30] J.-T. Bu, J.-Q. Zhang, G.-Y. Ding, J.-C. Li, J.-W. Zhang, B. Wang, W.-Q. Ding, W.-F. Yuan, L. Chen, Q. Zhong *et al.*, Chiral quantum heating and cooling with an optically controlled ion, Light Sci. Appl. **13**, 143 (2024).

[31] L. Feng, R. El-Ganainy, and L. Ge, Non-Hermitian photonics based on parity–time symmetry, Nature Photon **11**, 752 (2017).

[32] A. Li, H. Wei, M. Cotrufo, W. Chen, S. Mann, X. Ni, B. Xu, J. Chen, J. Wang, S. Fan *et al.*, Exceptional points and non-Hermitian photonics at the nanoscale, Nat. Nanotechnol. **18**, 706 (2023).

[33] G. Harari, M. A. Bandres, Y. Lumer, M. C. Rechtsman, Y. D. Chong, M. Khajavikhan, D. N. Christodoulides, and M. Segev, Topological insulator laser: theory, Science **359**, eaar4003 (2018).

[34] Z. Gong, Y. Ashida, K. Kawabata, K. Takasan, S. Higashikawa, and M. Ueda, Topological phases of non-Hermitian systems, Phys. Rev. X **8**, 031079 (2018).

[35] E. J. Bergholtz, J. C. Budich, and F. K. Kunst, Exceptional topology of non-Hermitian systems, Rev. Mod. Phys. **93**, 015005 (2021).

[36] N. Okuma and M. Sato, Non-Hermitian topological phenomena: A review, Annu. Rev. Condens. Matter Phys. **14**, 83 (2023).

[37] F. Minganti, A. Miranowicz, R. W. Chhajlany, and F. Nori, Quantum exceptional points of non-Hermitian hamiltonians and liouvillians: The effects of quantum jumps, Phys. Rev. A **100**, 062131 (2019).

[38] M. A. Nielsen and I. L. Chuang, *Quantum Computation and Quantum Information* (Cambridge University Press, 2010).

[39] S. Cialdi, M. A. C. Rossi, C. Benedetti, B. Vacchini, D. Tamascelli, S. Olivares, and M. G. A. Paris, All-optical quantum simulator of qubit noisy channels, Appl. Phys. Lett. **110**, 081107 (2017).

[40] P. Renault, J. Nokkala, G. Roeland, N. Y. Joly, R. Zambrini, S. Maniscalco, J. Piilo, N. Treps, and V. Parigi, Experimental optical simulator of reconfigurable and complex quantum environment, PRX Quantum **4**, 040310 (2023).

[41] R. Vasile, F. Galve, and R. Zambrini, Spectral origin of non-markovian open-system dynamics: A finite harmonic model without approximations, Phys. Rev. A **89**, 022109 (2014).

[42] H.-P. Breuer, E.-M. Laine, and J. Piilo, Measure for the degree of non-markovian behavior of quantum processes in open systems, Phys. Rev. Lett. **103**, 210401 (2009).

[43] J. Nokkala, F. Arzani, F. Galve, R. Zambrini, S. Maniscalco, J. Piilo, N. Treps, and V. Parigi, Reconfigurable optical implementation of quantum complex networks, New J. Phys. **20**, 053024 (2018).

[44] F. Di Colandrea, A. Babazadeh, A. Dauphin, P. Massignan, L. Marrucci, and F. Cardano, Ultra-long quantum walks via spin–orbit photonics, Optica **10**, 324 (2023).

[45] A. D'Errico, F. Cardano, M. Maffei, A. Dauphin, R. Barboza, C. Esposito, B. Piccirillo, M. Lewenstein, P. Massignan, and L. Marrucci, Two-dimensional topological quantum walks in the momentum space of structured light, Optica **7**, 108 (2020).

[46] R. Simon and N. Mukunda, Minimal three-component SU(2) gadget for polarization optics, Phys. Lett. A **143**, 165 (1990).

[47] A. Rubano, F. Cardano, B. Piccirillo, and L. Marrucci, Q-plate technology: a progress review [Invited], J. Opt. Soc. Am. B **36**, D70 (2019).

[48] Notice that setting $p = 1$ does not correspond to a noisy interaction, as in this case, the channel would deterministically act on the qubit state.

[49] D. F. V. James, P. G. Kwiat, W. J. Munro, and A. G. White, Measurement of qubits, Phys. Rev. A **64**, 052312 (2001).

[50] E. T. Campbell, B. M. Terhal, and C. Vuillot, Roads towards fault-tolerant universal quantum computation, Nature (London) **549**, 172 (2017).

[51] M. Frey, K. Funo, and M. Hotta, Strong local passivity in finite quantum systems, Phys. Rev. E **90**, 012127 (2014).

[52] R. Salvia, G. De Palma, and V. Giovannetti, Optimal local work extraction from bipartite quantum systems in the presence of Hamiltonian couplings, Phys. Rev. A **107**, 012405 (2023).

[53] R. Castellano, D. Farina, V. Giovannetti, and A. Acin, Extended local ergotropy, Phys. Rev. Lett. **133**, 150402 (2024).

[54] T. Yu and J. H. Eberly, Sudden death of entanglement, Science **323**, 598 (2009).

[55] G. Torlai, C. J. Wood, A. Acharya, G. Carleo, J. Carrasquilla, and L. Aolita, Quantum process tomography with unsupervised learning and tensor networks, Nat. Commun. **14**, 2858 (2023).

[56] F. Di Colandrea, N. Dehghan, A. D'Errico, and E. Karimi, Fourier quantum process tomography, npj Quantum Inf. **10**, 49 (2024).

[57] G. De Filippis, A. de Candia, G. Di Bello, C. A. Perroni, L. M. Cangemi, A. Nocera, M. Sassetti, R. Fazio, and V. Cataudella, Signatures of dissipation driven quantum phase transition in rabi model, Phys. Rev. Lett. **130**, 210404 (2023).

[58] G. Di Bello, A. Ponticelli, F. Pavan, V. Cataudella, G. De Filippis, A. de Candia, and C. A. Perroni, Environment induced dynamical quantum phase transitions in two-qubit rabi model, Commun. Phys. **7**, 364 (2024).